

Electrochemical Simultaneously Determination of Phenol and o-Cresol in Water Based on ZnO Nanosheets

Junyi Liu¹, Hua Huang^{1,2}, Sheng Zhong^{1,2}, Xichun She², Dulin Yin^{1,*}

¹ National & Local Joint Engineering Laboratory for New Petro-chemical Materials and Fine Utilization of Resources, College of Chemistry and Chemical Engineering, Hunan Normal University, Changsha 410081, China

² Hunan Changling Petrochemical S & T Developing Co. Ltd, Yueyang 414012, China

*E-mail: dulinyin2015@126.com

Received: 25 February 2016 / Accepted: 16 March 2016 / Published: 1 April 2016

Phenol and o-cresol are two organic contaminants largely produced by many industries and could potentially harmful people and environment. In this study, we proposed an electrochemical approach that could simultaneously determination of phenol and o-cresol. This method contained a commercial electrode surface modification process that deposition of ZnO nanosheets on the screen printed electrode (SPE). The fabricated sensor exhibited an outstanding electrocatalytic performances toward electro-oxidation of phenol and o-cresol. After optimization of the detection condition, the detection range and detection limit of the sensor were determined. Moreover, the proposed sensor also successfully applied for detecting phenol and o-cresol on the real wastewater.

Keywords: Phenol; O-cresol; ZnO; Electrocatalysis; Sensor

1. INTRODUCTION

Phenol is a contaminant commonly produced in plastic, petrol, core, mining and food industries. It is commonly discharged as an effluent waste using sewage system. Studies showed that the phenol is a carcinogenic material which could has high risk related to the human health and environment. Therefore, the detection phenol is essential for many fields. As an organic pollutant, phenol cannot be biological treated due to the resistance by many micro-organisms. Irritating effect of skin, mucous membranes and eyes could occur when exposure to the phenol. The lethal dosage of the phenol for human is 1 g. A series of symptoms such as loss of coordination, respiratory arrest could occur when swallow the phenol. Therefore, the use of phenols is usually has been legislated [1]. Many

different methods have been developed for determination of phenol such chromatographic method [1], spectroscopy based method [2] and electrochemical methods [3-7].

Cresol is an organic material commonly used in many manufacture industries such as pesticide and antioxidants factories. As similar to the phenol, cresol also been discharged as an effluent waste using sewage system [8]. Cresol also can be accumulated in biological chain and harm human health [9, 10]. Therefore, many governments prescribe the legal limits of using cresol especially the discharge concentration of cresol in wastewater. For instance, the discharge standard limit of cresol in wastewater in China is 0.1 mg/L. Many different methods have been developed for treating cresol before discharge, such as Fenton oxidation [11], photocatalysis degradation [12], photo-electro assisted Fenton treatment [13], electrochemical oxidation [14-16] and ozone treatment [17]. However, the analytical determination methods for cresol still need to be improved.

Electrochemical method for electro-active substance determination is a superior detection method due to its quick sample preparation requirement, low cost, high accuracy and easy operation procedures. Recently, electrochemical determination of pollutant received a lot of attentions [18-25]. For example, Zhao and co-workers demonstrated a copper oxide-reduced graphene oxide for electrochemical determination of catechol organic pollutant [26]. Sakthinathan and co-workers demonstrated a phenol electrochemical sensor based on the activated screen printed carbon electrode [27]. Wang and co-workers demonstrated a quinoline electrochemical sensor based on boron doped diamond electrode [28]. Pavinatto and co-worker demonstrated a 17α -ethinylestradiol electrochemical sensor based on the layer-by-layer assembled chitosan and multi-walled carbon nanotube [29]. It can be seen that the electrode surface modification can effectively enhance the electrochemical performance of commercial electrode due to the intrinsic properties of the modifier. ZnO is a well-studied transition metal oxide and showed a promising performance towards electrochemical sensor fabrication. ZnO nanostructures have been used for many electrochemical sensor construction such as levodopa [30], norepinephrine [31], uric acid [32], captopril [33], Hg (II) [34] and hydrazine [35]. In this work, we demonstrated an electrodeposition method for ZnO nanosheets fabrication on a screen printed electrode (SPE). Different characterization methods have been employed for morphology and properties analysis. The fabricated ZnO/SPE was then successfully used for electrochemical simultaneous determination of phenol and o-cresol

2. EXPERIMENTS

2.1 Materials

Phenol, o-cresol, zinc nitrate hexahydrate were bought from Sigma-Aldrich. Phosphate buffer solution (PBS) with different concentrations was prepared by mixing 0.1 M KH_2PO_4 and K_2HPO_4 . All water used in the experiment was Milli-Q water. All other reagents used throughout the experiments were analytical grade.

2.2 Electrodeposition of ZnO nanosheets

ZnO nanosheets were deposited on a screen printed electrode (SPE) using electrodeposition method. The deposition was carried out at a CHI 660A electrochemistry working station. A Pt plate and a saturated calomel electrode (SCE) in the Luggin capillary were used as the auxiliary electrode and the reference electrode, respectively. The electrodeposition process was conducted at quartz made electrochemical reaction cell using HNO₃ (0.1 M) as electrolyte, zinc nitrate hexahydrate (0.1 M) as ZnO precursor and chronoamperometry as deposition method. The electrodeposition potential was set as -0.7 V with 2 minutes.

2.3 Characterization

The morphology of ZnO nanosheets was observed by a scanning electron microscope (SEM, Quanta 200, FEI Corporation, Holland). EDX analysis will be conducted using an energy-dispersive X-ray spectroscopy equipped on the SEM. The crystal data of the ZnO nanosheets was collected from 10° to 90° in 2θ by a XRD with Cu Kα radiation (X'Pert Pro, PANalytical). UV-vis spectra of samples were collected by UV-Vis spectroscopy (HALO RB-10, Dynamica) in the wavelength range from 250 to 700 nm.

2.4 Electrochemical determination of phenol and o-cresol

The electrochemical measurements of phenol and o-cresol were carried out using a conventional three electrodes system. ZnO nanosheets modified SPE was used as working electrode. A Pt plate and a saturated calomel electrode (SCE) in the Luggin capillary were used as the auxiliary electrode and the reference electrode, respectively. Bare SPE was used as control group after electro-activation in 0.1 M H₂SO₄ for 5 cycles CV scans (-1.0 V to 1.0 V). Determination of phenol and o-cresol using CV method was performed at 0.1M PBS (pH = 7) at scan range between 0.2 to 1.2 V using scan rate of 50 mV/s. Electrochemical impedance spectroscopy (EIS) measurements were conducted in the frequency of 10¹~10⁵ Hz with an amplitude of 5 mV using 5 mM [Fe(CN)₆]^{3-/4-} probe with 0.1 M KCl. Linear sweep voltammetry (LSV) was applied to analysis of the electrochemical determination and detection of limit of proposed ZnO nanosheets modified SPE. The scan range and scan rate used in LSV measurements was similar as the CV measurements. The accumulation step was performed before LSV scan for enhancing the current response.

3. RESULTS AND DISCUSSION

3.1 Characterization of ZnO nanosheets

The morphology of electrodeposited ZnO nanosheets was observed using SEM. Figure 1 shows the SEM images of electrodeposited ZnO nanosheets with different magnifications. Under low

magnification, the ZnO nanosheets showed an aligned with interlaced structure. Moreover, the ZnO nanosheets showed a uniform distribution with a porous structure, which is beneficial for electrochemical reaction taken place. Under high magnification condition, the length and thickness of the ZnO nanosheets can be estimated as 1 μm and 20 nm, respectively. Nitrate reduction results in formation of hydroxide ions and hence causes the precipitation of zinc hydroxide onto the cathodic electrode, which is finally dehydrated into ZnO. This mechanism of electrodeposition can be described as follows [36]:

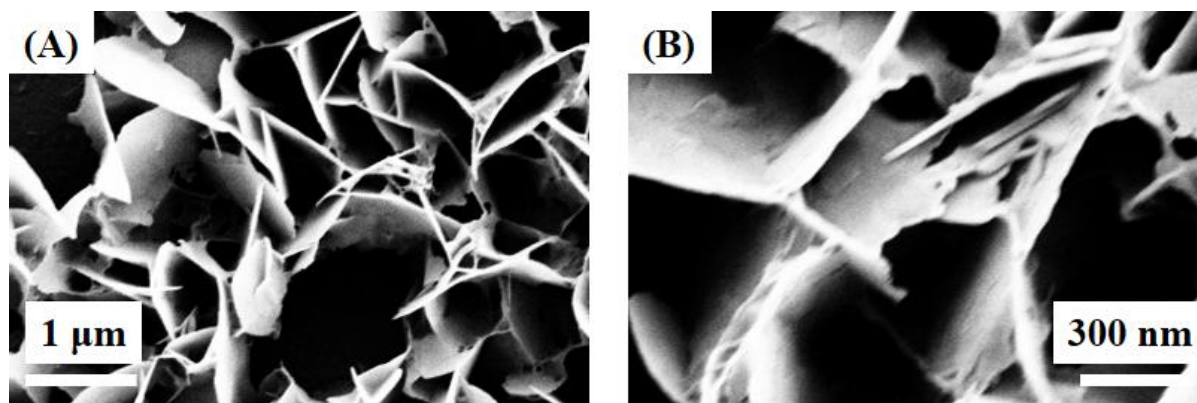
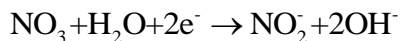


Figure 1. SEM images of ZnO nanosheets under (A) low magnification and (B) high magnification.

Figure 2A. As shown in the figure, the sample exhibits diffraction peaks at 32.1° , 34.5° , 36.2° , 47.5° , 56.5° , 62.3° and 68.2° corresponded to the (100), (002), (101), (102), (110), (103), (112) crystal phase, which can be assigned to hexagonal phase of ZnO (JCPDS 36-1451). Therefore, the growth of the ZnO nanosheets under -0.7 V condition is preferred in (101) direction. Moreover, no other impurity peak was observed in the XRD, suggesting the proposed electrodeposition method could form high purity of ZnO. The purity of the prepared ZnO nanosheets was also confirmed by EDX analysis. As shown in the Figure 2B, the spectrum of the ZnO nanosheets displays the only existence of O and Zn, further suggesting the successful formation of the ZnO nanosheets with high purity.

The crystal information of the ZnO nanosheets was collected using XRD and presented in Figure 2C shows the UV-vis spectrum of the electrodeposited ZnO nanosheets. The reflectance has the typical edge associated with the direct absorption of II–VI semiconductor materials. It can be observed that the spectrum exhibits a characteristic absorption peak at wavelength number of 388nm, suggesting the formed ZnO nanosheets had a high crystallization. Figure 2D shows the plots of the Kubelka-Munk remission function (relationship of $(\alpha h\nu)^2$ vs. photon energy) for ZnO nanosheets. The band gap of the formed ZnO nanosheets can be defined as 3.09 eV. This value agrees well with the literature value of the electrodeposited ZnO and is always attributed to the good crystallinity [37-40].

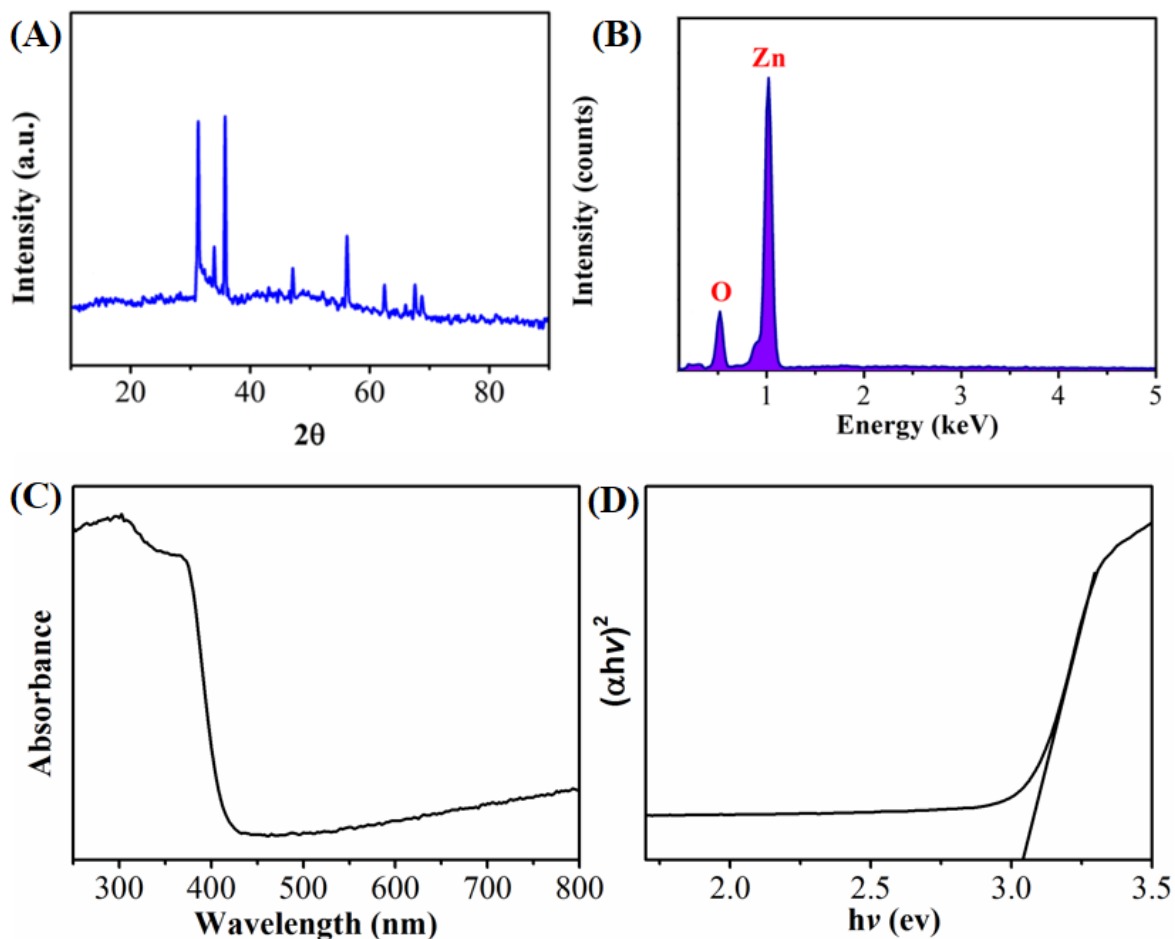


Figure 2. (A) XRD and (B) EDX spectrum of electrodeposited ZnO nanosheets. (C) UV-vis absorption spectrum and (D) plots of $(\alpha h\nu)^2$ vs. photon energy ($h\nu$) of electrodeposited ZnO nanosheets.

3.2 Electrochemical determination of phenol and *o*-cresol using ZnO/SPE

Figure 3A shows the cyclic voltammograms (CVs) of the bare SPE and ZnO nanosheets modified SPE towards electro-oxidation of 10 μM phenol. A small peak was observed on the bare SPE after 1.1 V due to the oxidation of phenol, while a much significant peak was observed on the ZnO nanosheets modified SPE at 0.8 V. The CV scan of ZnO nanosheets modified SPE when the absence of phenol confirmed the previous peak indeed related to the oxidation of phenol. On the other hand, the CVs of bare SPE and ZnO nanosheets modified SPE towards electro-oxidation of *o*-cresol were also studied. As shown in the Figure 3B, the bare SPE shows negligible current response towards *o*-cresol detection while the ZnO nanosheets modified SPE exhibits a distinct oxidation peak at 0.62 V with current of 37.5 μA . The current responses of phenol and *o*-cresol oxidation at ZnO nanosheets modified SPE almost 23 times and 34 times higher than that of the bare SPE, respectively. Figure 3C shows the simultaneous determination of phenol and *o*-cresol. The oxidation of phenol and *o*-cresol at ZnO nanosheets show clear over potential shift from 1.1 V to 0.8V and 1.18 V to 0.62 V, respectively.

Both observations indicate the electrocatalytic reaction was occurred on the ZnO nanosheets modified SPE and provided a better determination performance. The enhanced electrochemical performance towards phenol and o-cresol detection can be ascribed to the high surface of ZnO nanosheets, which provide an abundant sites for target molecules taken electrochemical reaction.

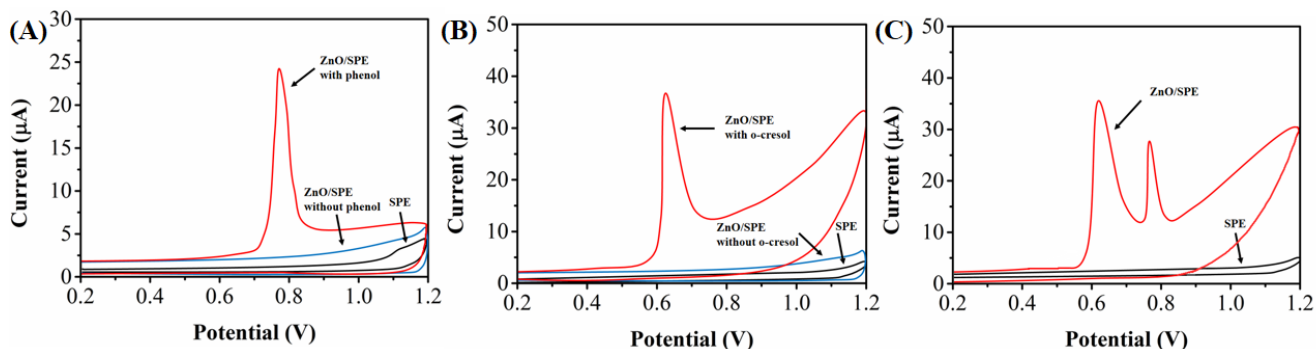


Figure 3. CVs profiles of bare SPE and ZnO/SPE towards detection of (A) phenol, (B) o-cresol and (C) both phenol and o-cresol in the 0.1 M PBS (pH 7.0). Scan rate: 50 mV/s.

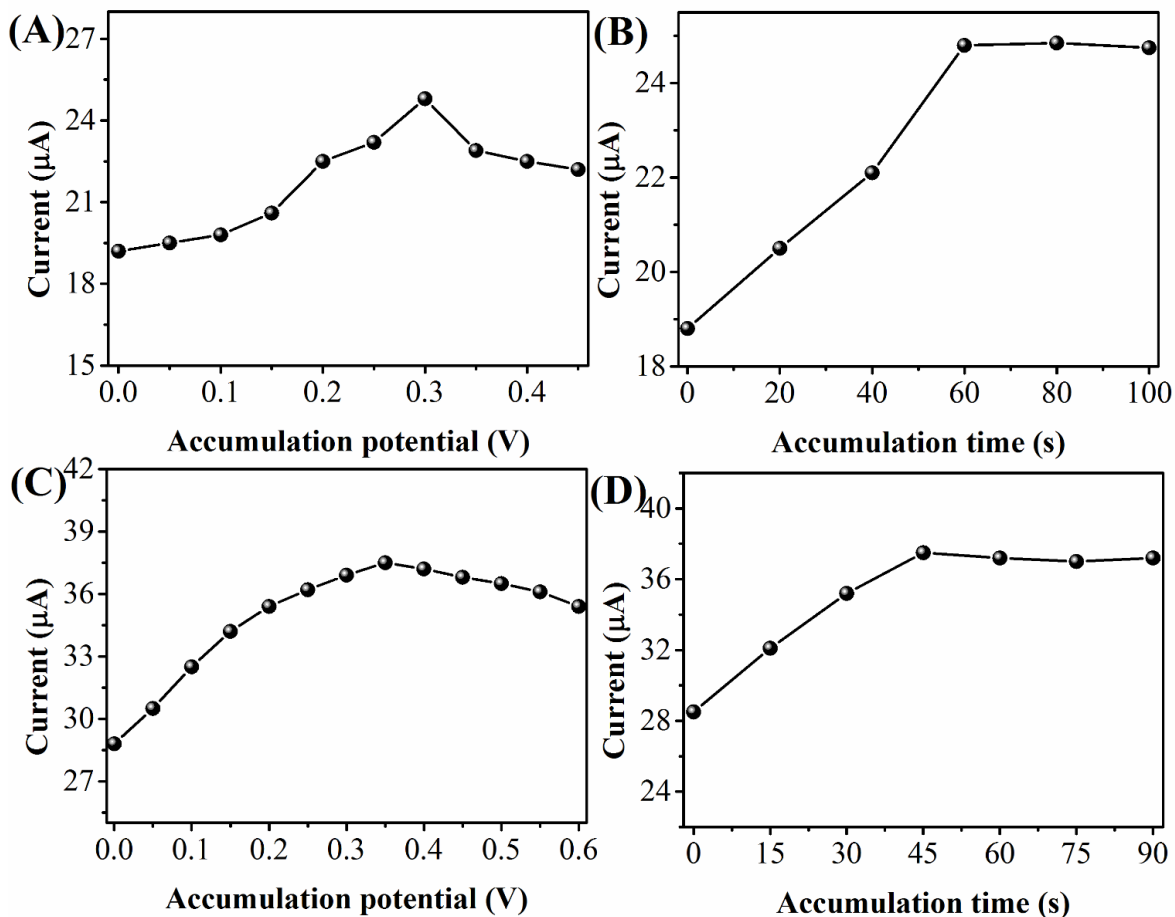


Figure 4. Effect of (A) Accumulation potential and (B) accumulation time on detection of phenol using ZnO nanosheets modified SPE. Effect of (C) Accumulation potential and (D) accumulation time on detection of o-cresol using ZnO nanosheets modified SPE.

Accumulation step was used for enhancing the current responses of the both phenol and o-cresol electro-oxidation. Figure 4A shows the effect of the accumulation potential on the current response of oxidation of phenol. It can be seen that the oxidation current of the phenol increased when the accumulation potential from 0 V to 0.3 V and then gradually reduced after further increasing the accumulation potential. Figure 4B shows the effect of the accumulation time on the current response of the oxidation of phenol. As shown in the figure, the peak current gradually increased when the accumulation time increased from 0 s to 60 s and then remains a similar current when further increased the accumulation. On the other hand, the effect of accumulation potential and time toward detection of o-cresol were displayed in Figure 4C and 4D, respectively. The best conditions for o-cresol detection was found to be 45 s accumulation time at 0.35 V. Consider the both results, the accumulation potential and accumulation time was set as 0.35 V and 60 s, respectively.

Under optimum condition, the analytical performance of the ZnO nanosheets was studied using linear sweep voltammetry (LSV) in 0.1 PBS. Figure 5A shows the LSV profiles of ZnO nanosheets modified SPE towards successive addition of phenol from 0.01 μM to 50 μM . A clear increasing of current response was observed when the phenol concentration increased. Inset of the Figure 5A shows the calibration curve of the relationship between current responses and concentrations. The linear regression equation can be expressed as: $I_{pa} (\mu\text{A}) = 2.189 c (\mu\text{M}) + 3.06668$ ($R^2 = 0.997$). The detection limit for phenol was then calculated to be 4.1 nM based on a signal to noise ratio of 3. Figure 5B shows the LSV profiles of ZnO nanosheets modified SPE towards successive addition of o-cresol from 0.01 μM to 50 μM . A similar trend was observed in this case as well. Inset of the Figure 5B displays the calibration curve of the relationship between current responses and o-cresol concentrations.

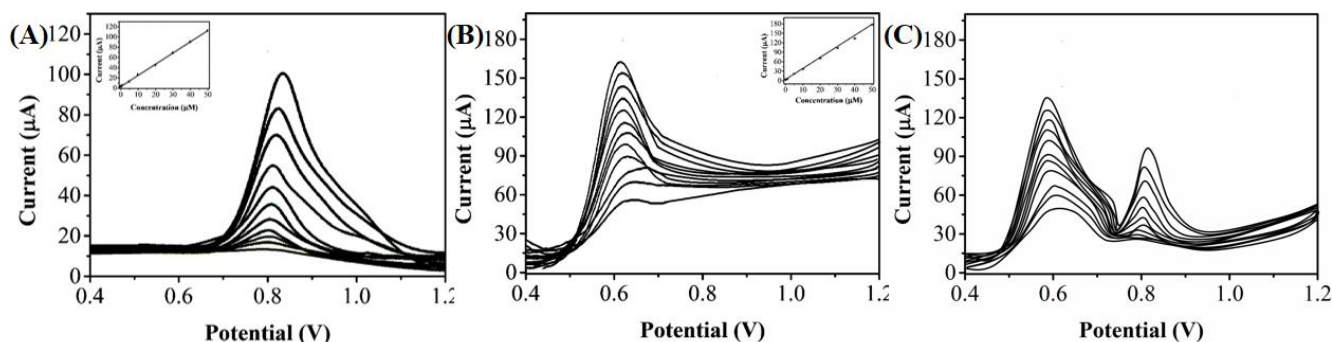


Figure 5. SLVs of ZnO/SPE toward detection of (A) phenol (0.01 μM to 50 μM), (B) o-cresol (0.01 μM to 50 μM) in PBS (pH=7.0) at scan rate of 50 mV/s. (C) SLVs of ZnO/SPE toward simultaneously determination of phenol and o-cresol at concentration range from 0.1 μM to 50 μM in PBS (pH=7.0) at scan rate of 50 mV/s.

The linear regression equation can be expressed as: $I_{pa} (\mu\text{A}) = 3.501 c (\mu\text{M}) + 4.21587$ ($R^2 = 0.995$). The detection limit for phenol was then calculated to be 5.5 nM based on a signal to noise ratio of 3. After individual test, the ZnO nanosheets modified SPE was then used for simultaneous determination of phenol and o-cresol. Figure 5C shows the performance of the ZnO nanosheets

modified SPE towards detection of both phenol and o-cresol in the concentration range from 0.1 μM to 50 μM . Two well-defined oxidation peaks were observed on the SLV profiles, indicating the ZnO nanosheets can be successfully used for detecting phenol and o-cresol at one time. Table 1 shows the comparison of our proposed phenol electrochemical sensor with some previous reported sensor. Although some reports showed a much larger determination range compared with our works [41, 42], they focused on the high concentration determination. Our proposed phenol sensor is more capable for trace amount of phenol detection. Moreover, our prepared phenol sensor did not involving polymer, which avoid the concerns of polymer degradation. On the other hand, the detection of o-cresol was rare reported in the literature. Therefore, our method provides a simple and quick approach for o-cresol detection.

Table 1. Comparison of our proposed electrochemical phenol sensor with previous reports.

Electrode	LDR (μM)	LOD (μM)	Reference
Tyrosinase/carbon black paste electrode	2-25	0.006	[43]
MWNT-Nafion- tyrosinase	1-19	0.13	[44]
Enzyme tyrosinase	0-0.629	0.0137	[45]
Gram-negative bacterial based sensor	—	5	[46]
Tyrosinase-ZnO	0.015-6.5	0.005	[47]
Platinum–polytyramine	300-10000	—	[41]
Polypyrrole and polyvinylpyrrolidone films	1-100	0.1	[42]
Boron-doped diamond film electrode	—	1.82	[48]
Poly azure B–clay–enzyme	0.004-18	0.004	[49]
Poly (N-3-aminopropyl pyrrole-co-pyrrole)- tyrosinase	1.35 –222.3	0.7	[50]
ZnO/SPE	0.01-50	0.0041	This work

4. CONCLUSIONS

In conclusion, ZnO nanosheets with high purity was synthesized using electrodeposition method. The synthesized ZnO sheets showed an aligned and interlaced structure with length and thickness of 1 μm and 20 nm, respectively. Moreover, the synthesized ZnO nanosheets modified SPE exhibited an outstanding performance towards simultaneous determination of phenol and o-cresol. The linear detection range of both target molecules was 0.01 μM to 50 μM . The detection limit of the phenol and o-cresol was 4.1 nM and 5.5 nM, respectively.

References

1. X. Zhou, J.P. Kramer, A.M. Calafat and X. Ye, *Journal of Chromatography B*, 944 (2014) 152
2. N. Zain, N.A. Bakar, S. Mohamad and N.M. Saleh, *Spectrochimica Acta Part A: Molecular and Biomolecular Spectroscopy*, 118 (2014) 1121
3. H. Beitollahi, S. Tajik and P. Biparva, *Measurement*, 56 (2014) 170

4. M.N. Karim and H.J. Lee, *Talanta*, 116 (2013) 991
5. Z. Mojović, N. Jović-Jovičić, A. Milutinović-Nikolić, P. Banković, A.A. Rabi-Stanković and D. Jovanović, *J. Hazard. Mater.*, 194 (2011) 178
6. G. Gao and C.D. Vecitis, *Electrochimica Acta*, 98 (2013) 131
7. B.C. Janegitz, R.A. Medeiros, R.C. Rocha-Filho and O. Fatibello-Filho, *Diamond and Related Materials*, 25 (2012) 128
8. D. Rajkumar, K. Palanivelu and N. Balasubramanian, *Journal of Environmental Engineering and Science*, 4 (2005) 1
9. J. Bai, J.-P. Wen, H.-M. Li and Y. Jiang, *Process Biochemistry*, 42 (2007) 510
10. P. Saravanan, K. Pakshirajan and P. Saha, *Bioresource Technology*, 99 (2008) 8553
11. V. Kavitha and K. Palanivelu, *Water. Res.*, 39 (2005) 3062
12. C. Gómez, G. Del Angel, F. Tzompantzi, R. Gómez and L. Torres-Martínez, *Journal of Photochemistry and Photobiology A: Chemistry*, 236 (2012) 21
13. C. Flox, P.-L. Cabot, F. Centellas, J.A. Garrido, R.M. Rodríguez, C. Arias and E. Brillas, *Appl. Ctatl. B-Environ.*, 75 (2007) 17
14. D. Rajkumar and K. Palanivelu, *Ind. Eng. Chem. Res.*, 42 (2003) 1833
15. C. Flox, C. Arias, E. Brillas, A. Savall and K. Groenen-Serrano, *Chemosphere*, 74 (2009) 1340
16. C. Flox, E. Brillas, A. Savall and K. Groenen-Serrano, *Current Organic Chemistry*, 16 (2012) 1960
17. M.C. Valsania, F. Fasano, S.D. Richardson and M. Vincenti, *Water. Res.*, 46 (2012) 2795
18. Y. Zheng, A. Wang, H. Lin, L. Fu and W. Cai, *RSC Advances*, 5 (2015) 15425
19. Y. Zheng, L. Fu, A. Wang and W. Cai, *Int. J. Electrochem. Sci.*, 10 (2015) 3530
20. L. Fu, Y.-H. Zheng and Z.-X. Fu, *Chemical Papers*, 69 (2015) 655
21. L. Fu, Y. Zheng, A. Wang, W. Cai and H. Lin, *Food chemistry*, 181 (2015) 127
22. L. Fu, Y. Zheng and A. Wang, *Int. J. Electrochem. Sci.*, 10 (2015) 3518
23. L. Fu, S. Yu, L. Thompson and A. Yu, *RSC Advances*, 5 (2015) 40111
24. L. Fu, G. Lai and A. Yu, *RSC Advances*, 5 (2015) 76973
25. L. Fu, G. Lai, P.J. Mahon, J. Wang, D. Zhu, B. Jia, F. Malherbe and A. Yu, *RSC Advances*, 4 (2014) 39645
26. Y. Zhao, X. Song, Q. Song and Z. Yin, *CrystEngComm*, 14 (2012) 6710
27. S. Sakthinathan, S. Palanisamy, S.-M. Chen, P.-S. Wu, L. Yao and B.-S. Lou, *Int. J. Electrochem. Sci.*, 10 (2015) 3319
28. C. Wang, K. Ma, T. Wu, M. Ye, P. Tan and K. Yan, *Chemosphere*, 149 (2016) 219
29. A. Pavinatto, L.A. Mercante, C.S. Leandro, L.H. Mattoso and D.S. Correa, *Journal of Electroanalytical Chemistry*, 755 (2015) 215
30. A. Afkhami, F. Kafrashi and T. Madrakian, *Ionics*, 21 (2015) 2937
31. Y. Wang, S. Wang, L. Tao, Q. Min, J. Xiang, Q. Wang, J. Xie, Y. Yue, S. Wu and X. Li, *Biosensors and Bioelectronics*, 65 (2015) 31
32. L. Fu, Y. Zheng, A. Wang, W. Cai, B. Deng and Z. Zhang, *Arab J Sci Eng*, 41 (2016) 135
33. H. Beitollahi, S. Ghofrani Ivvari, R. Alizadeh and R. Hosseinzadeh, *Electroanalysis*, 27 (2015) 1742
34. Y. Zhuang, J. Sun and Y. Guan, *Int. J. Electrochem. Sc.*, 10 (2015) 5961
35. R. Madhu, B. Dinesh, S.-M. Chen, R. Saraswathi and V. Mani, *RSC Advances*, 5 (2015) 54379
36. K. Peng, Y. Wu, H. Fang, X. Zhong, Y. Xu and J. Zhu, *Angewandte Chemie International Edition*, 44 (2005) 2737
37. M. Dai, F. Xu, Y. Lu, Y. Liu and Y. Xie, *Appl. Surf. Sci.*, 257 (2011) 3586
38. F. Xu, Y. Lu, Y. Xie and Y. Liu, *Vacuum*, 83 (2008) 360
39. F.A. Cataño, H. Gomez, E.A. Dalchiele and R.E. Marotti, *Int. J. Electrochem. Sci.*, 9 (2014) 534
40. P.B. Ozden, Y. Caglar, S. Ilican and M. Caglar, *Journal of Nanoelectronics and Optoelectronics*, 11 (2016) 244

41. T. Spătaru and N. Spătaru, *J. Hazard. Mater.*, 180 (2010) 777
42. Z. Chen and M. Hojo, *Bunseki Kagaku*, 56 (2007) 669
43. S. Nadifiyine, M. Haddam, J. Mandli, S. Chadel, C.C. Blanchard, J.L. Marty and A. Amine, *Analytical Letters*, 46 (2013) 2705
44. Y.-C. Tsai and C.-C. Chiu, *Sensors and Actuators B: Chemical*, 125 (2007) 10
45. J. Adamski, P. Nowak and J. Kochana, *Electrochimica Acta*, 55 (2010) 2363
46. A. Makarenko, I. Bezverbnaya, I. Kosheleva, T. Kuvichkina, P. Il'yasov and A. Reshetilov, *Applied biochemistry and microbiology*, 38 (2002) 23
47. Y.-F. Li, Z.-M. Liu, Y.-L. Liu, Y.-H. Yang, G.-L. Shen and R.-Q. Yu, *Analytical Biochemistry*, 349 (2006) 33
48. G.H. ZHAO, Y.T. TANG, M.C. LIU, Y.Z. LEI and X.E. XIAO, *Chinese Journal of Chemistry*, 25 (2007) 1445
49. D. Shan, C. Mousty, S. Cosnier and S. Mu, *Journal of Electroanalytical Chemistry*, 537 (2002) 103
50. Rajesh, W. Takashima and K. Kaneto, *Sensors and Actuators B: Chemical*, 102 (2004) 271

© 2016 The Authors. Published by ESG (www.electrochemsci.org). This article is an open access article distributed under the terms and conditions of the Creative Commons Attribution license (<http://creativecommons.org/licenses/by/4.0/>).